ACS APPLIED MATERIALS & INTERFACES

Research Article

www.acsami.org

Improved Adhesion Between PMMA and Stainless Steel Modified with PMMA Brushes

Kyoko Shimizu,*[,†] Kristoffer Malmos,[‖] Allan Hjarbæk Holm,[‖] Steen Uttrup Pedersen,[†,‡] Kim Daasbjerg,[†,‡] and Mogens Hinge*[,§]

[†]Department of Chemistry, [‡]Interdisciplinary Nanoscience Center (iNANO), Department of Physics and Astronomy, and [§]Department of Engineering, Aarhus University, Aarhus, Denmark

[‖]Grundfos Holding A/S, Poul Due Jensens Vej 7, DK-8850 Bjerringbro, Denmark

Supporting Information

ABSTRACT: In this work, various lengths and densities of poly(methyl methacrylate) (PMMA) brushes were synthesized on stainless steel (SS) surfaces via surface initiated atom transfer radical polymerization. Subsequently, the joints between the bulk PMMA and the PMMA brushed stainless steel were obtained by injection molding, and for these the degree of adhesion was assessed by tensile testing. Several conditions are required to facilitate the mixing between the brushes and the bulk polymer and to reduce the residual stress at the interface: preheating of the SS samples before the injection molding; a long packing time; and a mold temperature above the glass transition temperature (T_g) of PMMA during the injection molding. This treatment leads to a cohesive failure in the bulk PMMA. It was observed that the stress concentrated at the rim, due to contraction of bulk PMMA during cooling, results in a weak adhesion at the rim of the joint. A combination of high density and long brush length of PMMA film provides better adhesion. The large number of PMMA brush chains apparently promotes good penetration into the bulk PMMA chains and ultimately results in high adhesion strength.

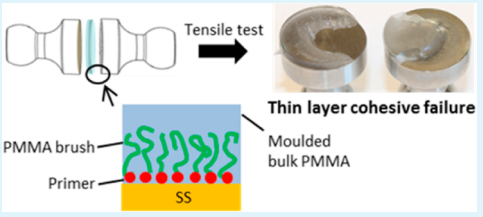

KEYWORDS: *adhesion, poly(methyl methacrylate), surface-initiated atom transfer radical polymerization, polymer brush, injection molding, X-ray photoelectron spectroscopy*

1. INTRODUCTION

Structural adhesive bonding is applied widely across most industrial sectors, for example, automotive, electronics, and coating industries.[1] The modification of surfaces and tailoring of surface properties with organic films have recently received a large amount of interest since this may improve the surface interaction with surrounding media.[2,3] The main concern when applying an adhesive is the in-service durability of the resulting connections under a range of conditions. The durability of the adhesive bonds can be improved by ensuring covalent bonds between the plastic item/coating and the underlying material, for example, a metallic surface.[2−5] A convenient way to obtain covalent bonds with metallic surfaces is by employing the electrofacilitated reduction of aryldiazonium salts using the metal as cathode.[2,3,6] The process results in the anchoring of an organic layer, and the new surface can be applied either as-prepared[7,8] or after another modification, to interact with the desired plastic item or topcoat.[9−11]

In this paper the approach was to generate the anchored organic layer by covalently linking polymer brushes to the surface utilizing a surface-immobilized initiator, thus, a "grafting from" approach.[3,12−15] As the polymer brushes are miscible with the incoming bulk polymer then mixing and/or entanglement of the surface-confined polymer brushes into the bulk polymer is expected. The result is a polymer−polymer mixing zone, the nature of which depends on the brush length, time, temperature, and thermodynamic driving force.[16,17] For alike/same polymers, entropy is the main driving force for mixing of the surface-immobilized polymer brushes into the bulk polymer melt. The surface density and length of individual chains of polymer brushes, along with the relative ratio of these, are important for the extent of interpenetration of polymer brushes into the bulk polymer.[18−21] In general, long polymer chains at an appropriate density are necessary to obtain good interpenetration and thereby good adhesion, due to the ability of sufficiently long polymer chains to entangle with the chains of the adhering polymer.[19,20,22,23] In the low-density regime, the grafted chains are isolated from one another and have freedom to move and interpenetrate into a polymer melt, and thus adhesion improves, at least up to a certain cutoff value of the graft density. Beyond this cutoff value adhesion decreases due to decreasing flexibility of the polymer chains, which have lower free volume. As the surface density continues to increase, the grafted chains begin to overlap and phase separate from the polymer melt, and interpenetration of the grafted chains into the polymer melt decreases even further.[20,23]

The objective of this work is to investigate the adhesion between a chemically modified SS surface and a bulk polymer

Received: September 13, 2014
Accepted: October 28, 2014
Published: October 28, 2014

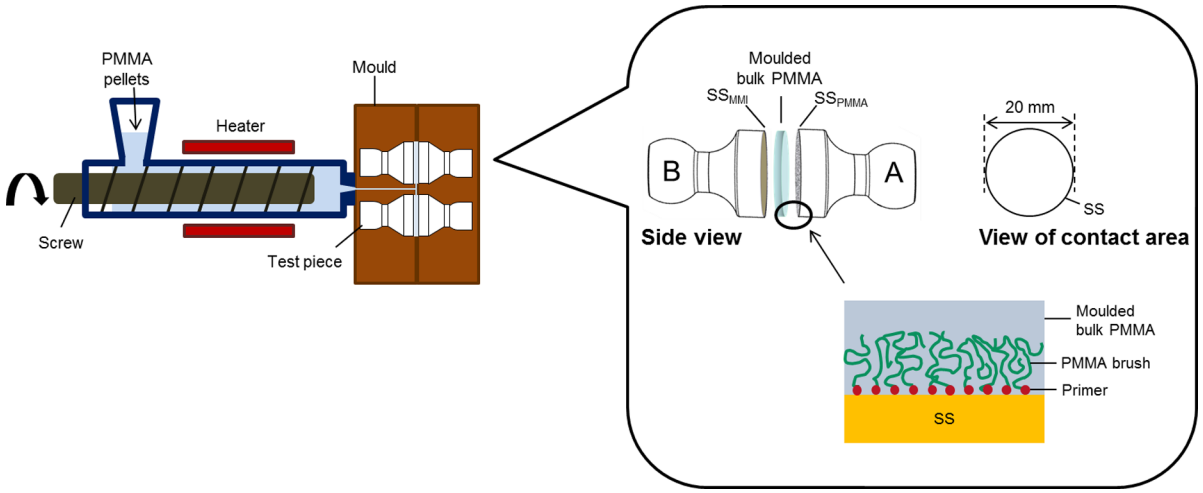

Figure 1. Schematic of the tensile strength test sample fabrication where (A) was SS_{PMMA}^{Y} and (B) was SS_{MMI}. The bulk PMMA is sandwiched between the SS_{MMI} and SS_{PMMA}^{Y} by injection molding.

Table 1. Experimental Conditions Used for Surface Modifications, Dry Film Thickness, Injection Molding Conditions, and Tensile Strength

entry	joint SS (A) samples	HEBD/ mM	BIBB/ mM	acylation time/h	%Br	dry film thickness/ nm	PMMA melt T/°C	mold T/°C	packing time/s	strength/ MPa
1	SS_{MMI}						240	60[a]	15	0.5 ± 0.0
2	SS_{MMI}						260	120	300	13 ± 2
3	SS_{Blank}						260	120	60	0
4	SS_{Blank}						260	120	300	2 ± 2
5	SS_{PMMA}^{I}	2.0	500	3		28 ± 6	260	120	60	2 ± 1
6	SS_{PMMA}^{I}	2.0	500	3		28 ± 6	260	120	180	3.5 ± 1
7	SS_{PMMA}^{I}	2.0	500	3		28 ± 6	260	120	300	5 ± 1
8	SS_{PMMA}^{II}	3.3	5	0.25	0.7	5 ± 2	260	120	300	6 ± 2
9	SS_{PMMA}^{III}	3.3	50	0.5	1.5	12 ± 4	260	120	300	5 ± 1
10	SS_{PMMA}^{IV}	3.3	300	1	1.8	43 ± 3	260	120	300	8 ± 2
11	SS_{PMMA}^{V}	3.3	500	3	2.9	34 ± 4	260	120	300	6.5 ± 1

[a] SS_{MMI} sample was not preheated at 100 °C.

as a function of variable graft density. Hence, a series of samples with various graft densities were synthesized by adjusting the reaction time and concentration of initiator solution.[24,25] Covalently attached poly(methyl methacrylate) (PMMA) was then formed on SS by surface-initiated atom transfer radical polymerization (SI-ATRP).[24] The polymerization was verified and quantified by infrared reflection adsorption spectroscopy (IRRAS). The SS and the bulk polymer junctions were then created with a range of parameters such as various injection molding conditions and the chain lengths and densities of the surface-immobilized PMMA brushes. Mechanical testing then allows a determination of the ultimate tensile strength of the interface. Finally, to investigate the failure mechanism and locus of failure, X-ray photoelectron spectroscopy (XPS) was applied.

2. MATERIALS AND METHODS

2.1. Materials. Ethanol (96%, VWR International), acetone (99%, VWR International), acetonitrile (MeCN) (HLPC grade, Aldrich), dichloromethane (DCM) (HLPC grade, Aldrich), 2-bromoisobutyryl bromide (BIBB) (98%, Aldrich), *N*,*N*,*N*′,*N*″,*N*″-pentamethyldiethylenetriamine (PMDETA) (99%, Aldrich), triethylamine (TEA) (>99%, Aldrich), $Cu^{I}Cl$ (>98%, Merck), and $Cu^{II}Cl_2{\cdot}2H_2O$ ((>99%, Merck) were used without further purification. The supporting electrolyte tetrabutylammonium tetrafluoroborate (Bu_4NBF_4) was prepared using standard procedure.[26] 4-(2-Hydroxyethyl)aniline (>98%, Aldrich) was used to synthesize 4-(2-hydroxyethyl)benzendiazonium tetrafluoroborate (HEBD), following standard synthesis procedures described elsewhere.[27] Methyl methacrylate (MMA) (99%, Aldrich) was passed through an aluminum oxide column to remove inhibitor. PMMA (DIAKON CLG902L) pellets (Lucite International, Inc.) were used for the injection molding.

Test pieces shaped according to ASTM D4541[28] with 20 mm diameter contact area were made of SS (ASTM 304) and are illustrated in Figure 1. The SS pieces were prepeared by abrading the contact surface using silicon carbide abrasive papers (P180, P500, and P1000) giving a roughness of approximately 30 μm. Afterward, the SS pieces were rinsed thoroughly with deionized water and ethanol followed by sonication in ethanol for 15 min.

Microstructured SS (SS_{MMI}) pieces, which can induce micromechanical interlocking (MMI) between the metal and the bulk polymer, were prepared to serve either as a mechanically interlocked counterpart or as a benchmark for the strength of the interface. The SS surface was prepared for MMI by laser structuring using a commercial Nd:YLF nanosecond laser with central wavelength of 1047 nm, a pulse energy of 1 mJ, and a repetition rate of 40 kHz. The laser light was focused onto the sample using an f = 250 nm lens giving a focused spot size of 48 μm leading to a peak intensity of 300 MW cm^{-2}. The SS type 1.4301 was employed and structured by 5 times 11 pulses into the same hole to yield a diameter and depth of approximately 100 μm for these holes. Holes were made with approximately 150 μm separation in a cubic pattern (Figure S1, Supporting Information).[29,30]

2.2. Electrografting and Preparation of Initiator Layer. The initiator layer was applied onto the SS test pieces following the electrografting protocol given in literature.[24] Briefly, the electro-

Scheme 1[a]

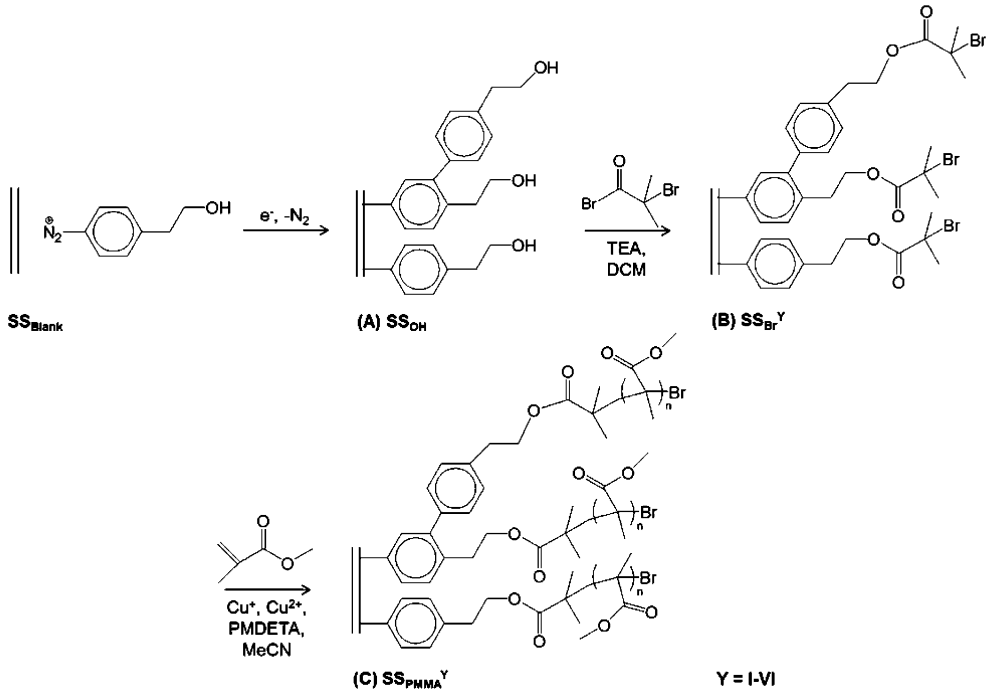

[a](A) Formation of a covalently attached initiator film on SS through electrografting of HEBD tetrafluoroborate to obtain the grafted substrate SS_{OH}. (B) The second step consists of a nucleophilic acyl substitution reaction with BIBB to form the corresponding initiator-based film, SS_{Br}^{Y} (Y = I–V, see Table 1. (C) SI-ATRP is employed using MMA as a monomer to produce covalently surface-attached polymer brushes, SS_{PMMA}^{Y}.

chemical modifications of the SS_{Blank} samples were performed by potentiostatic electrolysis in 2 or 3.3 mM HEBD and 0.1 M Bu_4NBF_4/MeCN for 60 s at a potential 0.4 V more negative than the voltammetric peak potential $E_{p,c}$, determined from an initial cyclic voltammetric sweep (sweep rate = 0.2 V s^{-1}) (Figure S2, Supporting Information). Subsequently, the hydroxyl-terminated SS samples (SS_{OH}) were immersed in DCM solution containing different concentrations of BIBB (5, 50, 300, and 500 mM) and 50 mM TEA at room temperature for different reaction times (0.25–3 h) to prepare the various initiator density samples, SS_{Br}^{Y} (Y = I–V, see Table 1 for details).

2.3. SI-ATRP Procedure. Solutions for SI-ATRP were degassed by a flow of argon through the sample for 20 min prior to polymerization. For all SI-ATRP, MMA (160 mL) in MeCN (4.7 M) solution was added into a 250 mL three-necked round-bottom flask and degassed. Subsequently, the ligand, PMDETA (0.2 mL, 10 mmol), catalyst, $Cu^{I}Cl$ (80.0 mg, 0.8 mmol), and deactivator $Cu^{II}Cl_2{\cdot}2H_2O$ (33.9 mg, 0.2 mmol) were degassed and introduced in the MMA solution, and the solution was stirred and degassed for additional 15 min (argon flow method). The SS_{Br}^{Y} was partially immersed into the reaction mixture and polymerized at 60 °C for 2 h under an inert argon atmosphere. Afterward, the samples were rinsed with acetone, followed by sonication in ethanol and acetone for 15 min in each solvent. The PMMA-modified SS are then denoted as SS_{PMMA}^{Y} (e.g., SS_{PMMA}^{I}).

Scheme 1 shows a summary of the procedure for preparation of the covalently attached PMMA brushes on the SS surfaces through the SI-ATRP technique. (A) Formation of a covalently attached initiator film on the SS is obtained through electrografting of HEBD tetrafluoroborate. (B) A nucleophilic acyl substitution reaction with BIBB formed the corresponding initiator-based film. (C) The SI-ATRP is employed, using MMA as a monomer, to produce covalently surface-attached polymer brushes.

2.4. Injection Molding. Injection molding was employed to cast the molten bulk PMMA onto the SS pieces and therefore make the joints. Figure 1 sketches the general setup with all relevant features. Illustrated joint samples consisted always of a SS_{MMI} piece (B) and an SS_{MMI}, SS_{Blank}, or SS_{PMMA}^{Y} piece (A). Injection molding with the SS_{PMMA}^{Y} samples was always conducted after preheating of both SS pieces at 100 °C for 90 min. Various injection molding parameters in terms of the temperature of the injected PMMA, the mold temperature, and the packing time were used and are summarized in Table 1.

2.5. Tensile Test. The tensile strength of polymer to metal joints was determined in accordance with ASTM D4541.[28] The ultimate tensile strength was determined using an Instron 5500R or Instron 4303 with a load cell of 25 kN at a crosshead speed of 0.1 mm/min.

2.6. Infrared Reflection Absorption Spectroscopy (IRRAS). IRRAS spectra were recorded on a Nicolet 6700 (Thermo Fisher Scientific). The Fourier transform infrared (FTIR) spectrometer was equipped with an external module, which had a narrow band mercury–cadmium–telluride (MCT) detector cooled with liquid nitrogen. The infrared beam was *p*-polarized by a gold wire polarizer. The spectral resolution and number of scans averaged were 4 cm^{-1} and 100, respectively. The SS samples were irradiated at an angle of 80°. The *p*-polarized reflectivity of the film, $R_p(d)$, was divided with reflectivity of the bare substrate $R_p(0)$ and presented as IRRAS absorbance $[-\log(R_p(d)/R_p(0))]$ after baseline correction using facilities of the OMNIC32 software. All spectra were recorded at room temperature under a dried atmosphere. The dry film thickness was calculated from a calibration curve using IRRAS absorbance values (Figure S2.2, Supporting Information).[24,31]

2.7. XPS. XPS analysis was achieved using a Kratos Axis Ultra-DLD spectrometer (Kratos Analytical Ltd., Manchester, U.K.). The analyzer was operated in the constant analyzer energy (CAE) mode at a pass energy = 160 eV for the survey spectra and a pass energy = 20 eV for high-resolution spectra of the elements of interest. Monochromated Al Kα X-ray at power = 150 W with an analysis area = 300 × 700 μm^2 was used. Charge compensation was achieved using an electron flood gun. The binding energy (BE) = 285.0 eV for C–C/C–H components of C 1s peak was used as reference for charge correction. Spectral processing was carried out using the computer software CasaXPS (v. 2.3.15) provided by Casa Software Ltd. (Teignmouth, U.K.).

3. RESULTS AND DISCUSSION

3.1. Characterization of PMMA Modified SS. The IRRAS absorbance pertaining to the ester C═O stretch band at 1740 cm^{-1} was collected along with the dry film thickness (Figures S3.1 and S3.2, Supporting Information), and the dry thickness is shown in Table 1.

Figure 2 shows a plot of the dry thickness of PMMA brushes against the %Br, which was obtained from XPS data (Table S4, Supporting Information). The dry-film thickness of the polymer brushes clearly depends on the surface concentration of Br. Our previous work has shown that a mushroom/pancake regime is obtained if the surface %Br does not reach a threshold value of = 0.16%.[24] Below this %Br the dry thickness is constant since the anchoring of the chains leaves sufficient space for the chains to grow and collapse onto the surface. Above the threshold %Br density the distance between two anchoring points becomes small enough, the polymer chains stretch away from the surface to minimize the interaction between themselves, and a brushlike conformation is formed.[18,24,32] In this study the %Br is always ≥0.7%, which means the brushes are in the stretch regime as indicated in Figure 2. Thus, as expected, the dry film thickness increases with increasing %Br content. A similar dry film thickness is found between the SS_{PMMA}^{IV} and SS_{PMMA}^{V}, which probably reflects the fact that fast biradical termination occurs, and only some of the initiators can grow high molecular weight polymer at the higher initiator density.[25,33] Thus, the dependence of the film growth rate on the initiator density is lower at higher initiator density.

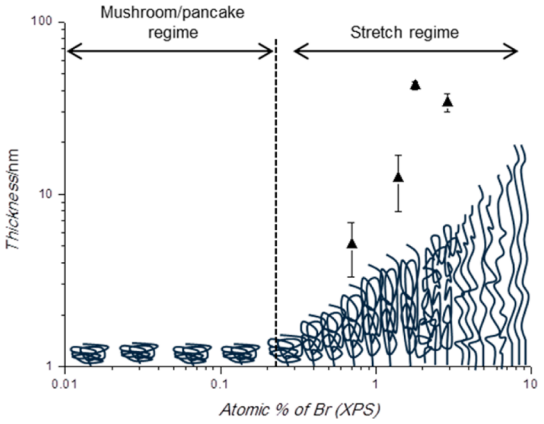

Figure 2. Atomic concentration of bromine on SS_{Br}^{Y} vs dry film thickness for SS_{PMMA}^{Y} (▲). The definition of the brush regimes are adapted from ref 24; however, the temperature and catalyst concentrations for ATRP differ from those used in this paper.

3.2. Parameter-Controlled Optimization of Injection Molding Condition. Injection molding was employed to produce a large number of reproducible test items for statistical evaluation. Table 1 provides an overview of the ultimate tensile strength of the different surface modifications and the injection molding parameters. First, various injection molding parameters in terms of the sample preheatment, the injection temperature, mold temperature, and the packing time were investigated using two SS_{MMI} test pieces (Table 1, entries 1 and 2). The tensile strength improved from 0.5 to 13 ± 2 MPa by increasing both PMMA melt and mold temperatures, probably due to lowering the viscosity of the melt resulting in a higher degree of the mechanical interlocking on the SS_{MMI} surfaces. As indicated above, significant improvements of the SS_{MMI} samples could be obtained not only by increasing the packing time to 300 s, but also by preheating at 100 °C for 90 min. So entries 1 and 2 represent the worst and best examples of adhesion between two SS_{MMI} samples. Additional experiments, which had varying injection and mold temperatures, showed almost no effect as long as the sample was not preheated and the packing times were less or equal to 60 s. Without preheating the polymer melt, it most probably solidified on the surface of the SS pieces without filling/packing the cavities in the MMI, and even if the sample is preheated the polymer melt still needs time to fill/pack the cavities.

3.3. Tensile Strength as a Function of the PMMA Brush Thickness. A series with the SS_{Blank} and SS_{PMMA}^{1} samples were tested (Table 1, entries 3−7). The tensile strength is improved from nonexistant (strength = 0 MPa) to 2 ± 2 MPa by increasing the packing time for the SS_{Blank} (entries 3−4), which is expected to be caused by the lowering of the interfacial residual stress. Thus, the packing time has a great influence on adhesion of the bulk PMMA to the SS_{Blank} surfaces.

No lasting adhesion was found between the bulk PMMA and SS_{PMMA}^{I} using a mold temperature lower than 120 °C (well above the glass transition temperature of the PMMA, T_g^{PMMA} = 105 °C).[34] Such a high mold temperature is probably required to ensure a significant and lasting joint, because of the structural relaxation in the cooling and packing.

Using a mold temperature of 120 °C, all SS_{PMMA}^{Y} samples exhibit higher tensile strength than SS_{Blank} samples, probably due to improved wetting of the surface toward the PMMA melt. The improved tensile strength with SS_{PMMA}^{I} from increasing the packing time (entries 5−7) suggests that the time for brush mixing with the polymer melt, particularly when above the T_g of the bulk polymer, is important. The kinetics of interdiffusion between polymer brushes and bulk polymer largely depend on the diffusion time.[17]

Additional experiments, not included in Table 1, which were carried out with similar SS_{Br}^{1} but with shorter PMMA brushes (dry-state thickness only 5 ± 3 nm), showed that a packing time of 60 s is sufficient to allow for interdiffusion of the short PMMA brushes and bulk PMMA; however, the interaction might be low, and the brush chains are pulled out resulting in a lower strength of 3 MPa.[20] By contrast, the longer chains of 28 ± 6 nm require longer time for the interdiffusion process but ultimately have a sufficient interaction leading to higher tensile strength, which might be caused by the inability of the chains to be pulled out of the bulk PMMA during the tensile test. The chain scission or crazing occurs, depending on the brush density.[20]

3.4. Adhesion as a Function of PMMA Brush Density. A range of samples with varying PMMA densities were compared in terms of the tensile strengths (Table 1, entries 8−11). In general, higher graft density tends to provide higher tensile strength. However, the significant standard deviations make it difficult to observe a clear trend. The SS_{PMMA}^{V} sample (entry 10) exhibits the highest strength (8 ± 2 MPa) for the PMMA-modified SS sample, although the values are still lower than the SS_{MMI} sample (entry 2) (13 ± 2 MPa).

Clearly, the tensile strength depends on the number of PMMA brushes and the extent of penetration. A high density of PMMA brushes ensures a larger number of chains are available for mixing with the bulk PMMA, while the opposite is expected for a low brush density. As a higher tensile strength of SS_{PMMA}^{IV} (entry 10) compared to that of SS_{PMMA}^{III} (entry 9) is observed,

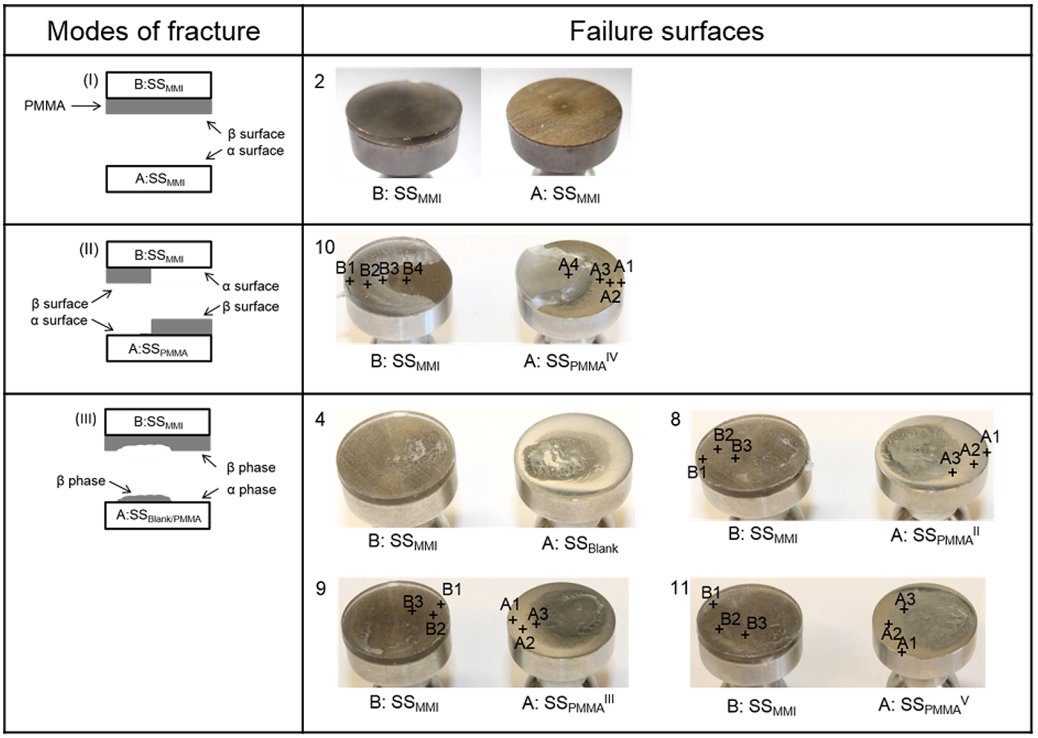

Figure 3. Failure surfaces (failure area of 20 mm diameter) of various samples after the tensile test. Three possible modes of separation of the joint: (I) Thin layer cohesive failure or interfacial failure at the bulk PMMA and SS_{MMI}. (II) Thin layer cohesive failure or interfacial failure at the bulk PMMA on both SS_{PMMA}^{IV} and SS_{MMI}. (III) Mix of cohesive failure and thin layer cohesive or interfacial failure at the bulk PMMA and SS_{blank} or SS_{PMMA}^{Y}. The α surface is defined as a failure surface of a thin (not apparent or visible) or completely absent PMMA layer, while the β surface is defined as a failure surface of a thick (visible) PMMA layer. Indicated regions (A1−A4 and B1−B4) are the sites of XPS analysis. For numbering system, see Table 1

it would imply that the brush density of SS_{PMMA}^{IV} is still sufficiently low to allow the chains enough flexibility and free volume to ensure a good interfacial mixing. The SS_{PMMA}^{V} sample (entry 11) shows lower strength than the SS_{PMMA}^{IV} sample (entry 10) and a lower PMMA thickness. It might be that the chains on the SS_{PMMA}^{V} are present in higher density compared to the SS_{PMMA}^{IV} thus indicating less freedom to move and thus less ability to interact with the bulk PMMA. On the other hand, the lower thickness is also expected to lead to a lower tensile strength.

3.5. Locus of Failure. Figure 3 shows the failure surfaces after the tensile test. In the case of the SS_{PMMA}^{IV} sample, the failure occurs at both bulk PMMA/SS_{MMI} and bulk PMMA/SS_{PMMA}^{IV} interfaces (entry 10). For other samples (entries 4, 8, 9, and 11), a thick bulk PMMA layer is present in the middle region of both sides of the failure surfaces, and thus the failure clearly occurs cohesively within the bulk PMMA. The apparent cohesive failure region, which represents approximately 30, 35, 40, and 47% of the area of the SS_{Blank}, SS_{PMMA}^{II}, SS_{PMMA}^{III}, and SS_{PMMA}^{V} failure surfaces, respectively, tends to increase with increasing graft density. On the rim, however, the failure modes tend to be near the bulk PMMA/SS_{PMMA}^{Y} or SS_{Blank} interface (by visual examination). This is in good agreement with a theory that stresses are concentrated on the edge region of the circular item due to the difference in thermal expansion coefficients of SS and PMMA (which are 1×10^{-5} K^{-1} and 7×10^{-5} K^{-1}, respectively,[35]) which leads to weak adhesion at the rim.[36] By contrast, low stress in the middle region, from stress relaxation, results in strong adhesion.[36,37] This stress distribution can initiate a crack propagation which results in a cohesive failure in the middle region.[19,22] By contrast, the crack formation was not observed on the SS_{MMI} sample. The SS_{MMI} sample seems to demonstrate an interfacial failure at the PMMA/SS_{MMI} interface. Presumably, this is due to the fact that the surface of the SS_{MMI} was laser structured, and thus the stress is concentrated on each groove rather than at the edge of the circular item.[38,39] XPS analysis was employed to identify the failure mode on these edge regions of the SS_{PMMA}^{Y}.

3.5.1. XPS Analysis of Failure Surfaces. Table 2 shows the results of the XPS analysis on both α and β surfaces of three different apparent interfacial failure regions; at the edge of the sample (A1 and B1), the outer region (A2 and B2), and the inner region (A3, A4, B3, and B4). The surface composition of the β surfaces of SS_{MMI} (B) pieces for all samples are generally closer to the theoretical values for PMMA, which are 71% carbon and 29% oxygen.

On α surfaces of all SS_{PMMA} (A) samples, the C/O ratio is always larger than the expected 2.4 for the bulk PMMA, and the deviation increases from the center (C/O = 3−6) to the edge region (C/O = 6−10). An increase in this ratio indicates a possible contribution of the primer layer, prepared with the electrochemical grafting process, since the primer layer has a higher C/O ratio compared with the PMMA layer (see Scheme 1). For the SS_{PMMA}^{II} sample, a small amount of iron is observed on the α surface of the edge region. This supports the observation that the failure occurs close to the bulk PMMA/SS_{PMMA}^{II} interface, and since the thickness of the PMMA brushes is only 4 nm, which is smaller than attenuation length of a photoelectron (approximately 10 nm), part of the underlying substrate is expected to be visible.

Figure 4 shows the high-resolution C 1s spectra of the SS_{PMMA}^{IV} samples at the α failure surfaces. PMMA has a

dx.doi.org/10.1021/am5062823 | ACS Appl. Mater. Interfaces 2014, 6, 21308−21315

Table 2. Surface Composition (atom %) of the Failure for Different Samples[a]

	C	O	C/O ratio
SS_{PMMA}^{II}			
A1 (α surface)[b]	85.1	14.6	5.8
A2 (α surface)	78.9	21.1	3.7
A3 (α surface)	82.7	17.3	4.8
B1 (β surface)	75.2	24.8	3.0
B2 (β surface)	73.7	26.3	2.8
B3 (β surface)	77.2	22.8	3.4
SS_{PMMA}^{III}			
A1 (α surface)	91.5	8.5	10.8
A2 (α surface)	90.0	10.0	9.0
A3 (α surface)	85.2	14.8	5.8
B1 (β surface)	83.5	16.5	5.1
B2 (β surface)	75.0	25.0	3.0
B3 (β surface)	73.8	26.2	2.8
SS_{PMMA}^{IV}			
A1 (α surface)	87.6	12.4	7.1
A2 (α surface)	83.9	16.1	5.2
A3 (α surface)	77.2	22.8	3.4
A4 (β surface)[c]	61.5	33.4	-
B1 (β surface)	76.1	23.9	3.2
B2 (β surface)	75.6	24.4	3.1
B3 (β surface)	76.0	24.0	3.2
B4 (α surface)[d]	78.4	18.9	-
SS_{PMMA}^{V}			
A1 (α surface)	90.9	9.1	10.0
A2 (α surface)	88.7	11.3	7.8
A3 (α surface)	79.7	20.3	3.9
B1 (β surface)	77.3	22.7	3.4
B2 (β surface)	76.0	24.0	3.2
B3 (β surface)	73.8	26.2	2.8

[a]Analysis area is indicated in Figure 3. Additional elements are detected (atom %). [b]Fe (0.3). [c]Fe (2.7), Cr (1.4), and Mn (1.1). [d]Fe (1.4), Cr (0.8), and Mn (0.7).

theoretical distribution of 40% of C−C and 20% of each of the *C−C(O)═O, C−O, and O−C═O components.[40] For the α surface (A3, Figure 4B) we find a distribution close to that for the bulk PMMA. By contrast, the α surface (A1, Figure 4A) of the edge region exhibits a high C−C component with low oxygenated functionalities, supporting the hypothesis that the signal has a substantial component from the primer layer in these regions. Similar trends are observed on the α surfaces of the other samples. The surface concentration of the SS_{PMMA}^{IV} sample was also analyzed by XPS before the injection molding and exhibits 74% carbon and 26% oxygen, indicating that the PMMA brush layer is thick enough to shield the primer layer from XPS detection. The fact that, after the injection molding and the tensile test, we observe contributions from the primer on the edge and at the outer regions must indicate that the failure does not occur at the bulk PMMA/PMMA brushes interface, but that it occurs in the PMMA brush layer or interdiffusion of the bulk PMMA/PMMA brushes layer, and in both cases the failure is close to the primer/SS substrate. Moreover, the locus of failure on the edge region is closer to the primer/SS substrate than at the outer region.

3.6. Failure Mechanism. Cohesive failure of the bulk PMMA in the middle region might have its origin in the stress alleviated by the thermal profile from the injection molding. The preheating time of 90 min at 100 °C and the packing time of 300 s at 120 °C must be long enough and high enough, respectively, to facilitate mixing of the brushes and the bulk polymer and also to release residual stress of the polymer at the interface.

By contrast, the failure on the edge region occurs very close to the PMMA brush/primer interface, at least within 10 nm, as judged from the escape depth of a photoelectron. The failure could result from either chain pullout or stress-related breakage due to the difference in the thermal expansion coefficients of SS and PMMA. Moreover, the shrinkage of PMMA (0.3−0.8%) by the thermal displacement may induce interfacial stress.

For the SS_{PMMA}^{IV} sample, the large number of PMMA brushes can make good penetration into the bulk PMMA and lead to relatively high tensile strength. In the case of the SS_{PMMA}^{II} sample, the bulk PMMA and PMMA brushes may also mix well; however, the number of cohesive interactions is lower, and this results in a lower strength. The rate of interdiffusion is difficult to examine since PMMA is used for both the bulk and the brushes, but the presence of the cohesive failure indicates a good interfacial mixing.

5. CONCLUSIONS

PMMA brushes covalently attached at a SS surface in various lengths and densities were injection overmolded with molten bulk PMMA. A tensile test was used to assess the strength of

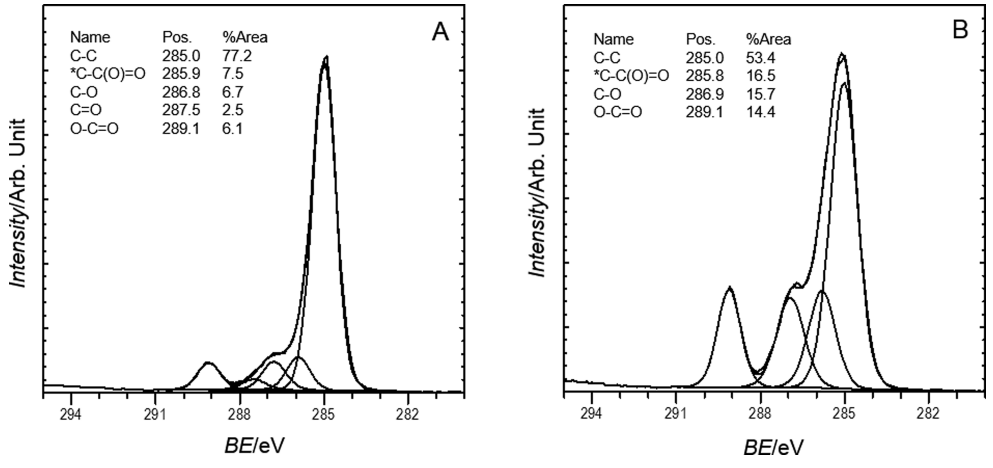

Figure 4. High-resolution of C 1s spectra of SS_{PMMA}^{IV} sample at the failure surface area of (A) A1 and (B) A3.

the interface between the bulk PMMA and the PMMA-modified SS. Preheating of samples at 100 °C for 90 min, a long packing time of 300 s, and a mold tool temperature of 120 °C, that is, above the T_g^{PMMA}, were needed to facilitate efficient mixing of brushes and bulk polymer while also alleviating residual stress of the polymer at the interface. Analysis of the failure area revealed a cohesive failure of the bulk PMMA on the central region. By contrast, high stress is concentrated at the rim by the shrinkage of PMMA during cooling and leads to a weak adhesion at the edge interface. Longer brushes and higher densities of the PMMA polymer brushes on the SS surfaces provide junctions with higher tensile strengths, probably because of deeper and more frequent penetration of the PMMA brushes into the bulk PMMA.

■ ASSOCIATED CONTENT

Supporting Information

SEM image of holes, description of electrografting experiment, IRRAS data, and XPS data. This material is available free of charge via the Internet at http://pubs.acs.org.

■ AUTHOR INFORMATION

Corresponding Authors

*Phone: +45 87155947. Fax: +45 86196199. E-mail: Shimizu@chem.au.dk. (K.S.)

*Phone: +45 22770555. Fax: +45 86196199. E-mail: hinge@eng.au.dk. (M.H.)

Notes

The authors declare no competing financial interest.

■ ACKNOWLEDGMENTS

The Danish Agency for Science, Technology and Innovation, Grundfos A/S and SP group A/S are gratefully acknowledged for financial support. Dr. S. Chernyy is acknowledged for ATRP-related data and discussion, Dr. M. Lillethorup is acknowledged for supplying data for the thickness calibration curve, and Dr. F. H. Blaikie is acknowledged for the proofreading.

■ REFERENCES

(1) Kneafsey, B. Structual Adhesives. In *Handbook of Adhesion,* 2nd ed.; Packham, D. E., Ed.; John Wiley & Sons: Chichester, West Sussex, 2005; pp 505−508.

(2) Belanger, D.; Pinson, J. Electrografting: a Powerful Method for Surface Modification. *Chem. Soc. Rev.* **2011**, *40*, 3995−4048.

(3) Mahouche-Chergui, S.; Gam-Derouich, S.; Mangeney, C.; Chehimi, M. M. Aryl Diazonium Salts: a New Class of Coupling Agents for Bonding Polymers, Biomacromolecules and Nanoparticles to Surfaces. *Chem. Soc. Rev.* **2011**, *40*, 4143−4166.

(4) Chaussé, A.; Chehimi, M. M.; Karsi, N.; Pinson, J.; Podvorica, F.; Vautrin-Ul, C. The Electrochemical Reduction of Diazonium Salts on Iron Electrodes. The Formation of Covalently Bonded Organic Layers and Their Effect on Corrosion. *Chem. Mater.* **2001**, *14*, 392−400.

(5) Sathyanarayana, M. N.; Yaseen, M. Role of Promoters in Improving Adhesions of Organic Coatings to a Substrate. *Prog. Org. Coat.* **1995**, *26*, 275−313.

(6) Pinson, J.; Podvorica, F. Attachment of Organic Layers to Conductive or Semiconductive Surfaces by Reduction of Diazonium Salts. *Chem. Soc. Rev.* **2005**, *34*, 429−439.

(7) Adenier, A.; Cabet-Deliry, E.; Lalot, T.; Pinson, J.; Podvorica, F. Attachment of Polymers to Organic Moieties Covalently Bonded to Iron Surfaces. *Chem. Mater.* **2002**, *14*, 4576−4585.

(8) Shimizu, K.; Malmos, K.; Spiegelhauer, S.-A.; Hinke, J.; Holm, A. H.; Pedersen, S. U.; Daasbjerg, K.; Hinge, M. Durability of PEEK Adhesive to Stainless Steel Modified with Aryldiazonium Salts. *Int. J. Adhes. Adhes.* **2014**, *51*, 1−12.

(9) Delamar, M.; Désarmot, G.; Fagebaume, O.; Hitmi, R.; Pinsonc, J.; Savéant, J. M. Modification of Carbon Fiber Surfaces by Electrochemical Reduction of Aryl Diazonium Salts: Application to Carbon Epoxy Composites. *Carbon* **1997**, *35*, 801−807.

(10) Sun, C.; Zhou, F.; Shi, L.; Yu, B.; Gao, P.; Zhang, J.; Liu, W. Tribological Properties of Chemically Bonded Polyimide Films on Silicon with Polyglycidyl Methacrylate Brush as Adhesive Layer. *Appl. Surf. Sci.* **2006**, *253*, 1729−1735.

(11) Shaulov, Y.; Okner, R.; Levi, Y.; Tal, N.; Gutkin, V.; Mandler, D.; Domb, A. J. Poly(methyl methacrylate) Grafting onto Stainless Steel Surfaces: Application to Drug-Eluting Stents. *ACS Appl. Mater. Interfaces* **2009**, *1*, 2519−2528.

(12) Matrab, T.; Chehimi, M. M.; Perruchot, C.; Adenier, A.; Guillez, A.; Save, M.; Charleux, B.; Cabet-Deliry, E.; Pinson, J. Novel Approach for Metallic Surface-Initiated Atom Transfer Radical Polymerization Using Electrografted Initiators Based on Aryl Diazonium Salts. *Langmuir* **2005**, *21*, 4686−4694.

(13) Lillethorup, M.; Kongsfelt, M.; Ceccato, M.; Jensen, B. B. E.; Jørgensen, B.; Pedersen, S. U.; Daasbjerg, K. High- versus Low-Quality Graphene: A Mechanistic Investigation of Electrografted Diazonium-Based Films for Growth of Polymer Brushes. *Small* **2014**, *10*, 922−934.

(14) Chen, F.; Jiang, X.; Liu, R.; Yin, J. Well-Defined PMMA Brush on Silica Particles Fabricated by Surface-Initiated Photopolymerization (SIPP). *ACS Appl. Mater. Interfaces* **2010**, *2*, 1031−1037.

(15) Chernyy, S.; Järn, M.; Shimizu, K.; Swerin, A.; Pedersen, S. U.; Daasbjerg, K.; Makkonen, L.; Claesson, P.; Iruthayaraj, J. Superhydrophilic Polyelectrolyte Brush Layers with Imparted Anti-Icing Properties: Effect of Counter ions. *ACS Appl. Mater. Interfaces* **2014**, *6*, 6487−6496.

(16) Kunz, K.; Stamm, M. Initial Stages of Interdiffusion of PMMA across an Interface. *Macromolecules* **1996**, *29*, 2548−2554.

(17) Schnell, R.; Stamm, M.; Creton, C. Direct Correlation between Interfacial Width and Adhesion in Glassy Polymers. *Macromolecules* **1998**, *31*, 2284−2292.

(18) Morita, H.; Miura, H.; Yamada, M.; Yamaguchi, T.; Doi, M. Molecular Dynamics Study of the Adhesion between End-Grafted Polymer Films II -Effect of Grafting Density-. *Polym. J. (Tokyo, Jpn.)* **2006**, *39*, 73−80.

(19) Léger, L.; Creton, C. Adhesion Mechanisms at Soft Polymer Interfaces. *Philos. Trans. R. Soc., A* **2008**, *366*, 1425−1442.

(20) Sides, S. W.; Grest, G. S.; Stevens, M. J.; Plimpton, S. J. Effect of End-Tethered Polymers on Surface Adhesion of Glassy Polymers. *J. Polym. Sci., Part B: Polym. Phys.* **2004**, *42*, 199−208.

(21) Gay, C. Wetting of a Polymer Brush by a Chemically Identical Polymer Melt. *Macromolecules* **1997**, *30*, 5939−5943.

(22) Creton, C.; Kramer, E. J.; Hui, C. Y.; Brown, H. R. Failure Mechanisms of Polymer Interfaces Reinforced with Block Copolymers. *Macromolecules* **1992**, *25*, 3075−3088.

(23) Gutowski, W. S. Interface/Interphase Engineering of Polymers for Adhesion Enhancement: Part I. Review of Micromechanical Aspects of Polymer Interface Reinforcement through Surface Grafted Molecular Brushes. *J. Adhes.* **2003**, *79*, 445−482.

(24) Iruthayaraj, J.; Chernyy, S.; Lillethorup, M.; Ceccato, M.; Røn, T.; Hinge, M.; Kingshott, P.; Besenbacher, F.; Pedersen, S. U.; Daasbjerg, K. On Surface-Initiated Atom Transfer Radical Polymerization Using Diazonium Chemistry to Introduce the Initiator Layer. *Langmuir* **2010**, *27*, 1070−1078.

(25) Bao, Z.; Bruening, M. L.; Baker, G. L. Control of the Density of Polymer Brushes Prepared by Surface-Initiated Atom Transfer Radical Polymerization. *Macromolecules* **2006**, *39*, 5251−5258.

(26) Scholz, F. *Electroanalytical Methods-Guide to Experiments and Applications;* Springer: Heidelberg, Germany, 2010.

(27) Starkey, E. B. *Organic Synthesis;* Wiley & Sons: New York, 1943; Vol. *2*

(28) International, A. *Standard ASTM D4541−09: Standard Test Method for Pull-off Strength of Coatings Using Portable Adhesion Testers;* ASTM International, 2009.
(29) Byskov-Nielsen, J.; Balling, P. Laser Structuring of Metal Surfaces: Micro-Mechanical Interlocking. *Appl. Surf. Sci.* **2009**, *255*, 5591−5594.
(30) Byskov-Nielsen, J.; Boll, J. V.; Holm, A. H.; Højsholt, R.; Balling, P. Ultra-High-Strength Micro-Mechanical Interlocking by Injection Molding into Laser-Structured Surfaces. *Int. J. Adhes. Adhes.* **2010**, *30*, 485−488.
(31) Lillethorup, M.; Torbensen, K.; Ceccato, M.; Pedersen, S. U.; Daasbjerg, K. Electron Transport through a Diazonium-Based Initiator Layer to Covalently Attached Polymer Brushes of Ferrocenylmethyl Methacrylate. *Langmuir* **2013**, *29*, 13595−13604.
(32) Wu, T.; Efimenko, K.; Genzer, J. Combinatorial Study of the Mushroom-to-Brush Crossover in Surface Anchored Polyacrylamide. *J. Am. Chem. Soc.* **2002**, *124*, 9394−9395.
(33) Kim, J.-B.; Bruening, M. L.; Baker, G. L. Surface-Initiated Atom Transfer Radical Polymerization on Gold at Ambient Temperature. *J. Am. Chem. Soc.* **2000**, *122*, 7616−7617.
(34) Saldivar-Guerra, E.; Vivaldo-Lima, E. *Handbook of Polymer Synthesis, Characterization, and Processing;* Wiley & Sons: Hoboken, NJ, 2013.
(35) Crawford, R. J. *Plastics Engineering,* 3rd ed; Elsevier Butterworth-Heinemann: Oxford, U.K., 1998.
(36) Kim, J. K.; Mai, Y. W. *Engineered Interfaces in Fiber Reinforced Composites,* Elsevier Science: Oxford, U.K., 1998.
(37) Priestley, R. D.; Ellison, C. J.; Broadbelt, L. J.; Torkelson, J. M. Structural Relaxation of Polymer Glasses at Surfaces, Interfaces, and In Between. *Science* **2005**, *309*, 456−459.
(38) Wasyluk, J.; Adley, D.; Perova, T. S.; Rodin, A. M.; Callaghan, J.; Brennan, N. Micro-Raman Investigation of Stress Distribution in Laser Drilled via Structures. *Appl. Surf. Sci.* **2009**, *255*, 5546−5548.
(39) Amer, M. S.; Dosser, L.; LeClair, S.; Maguire, J. F. Induced Stresses and Structural Changes in Silicon Wafers as a Result of Laser Micro-Machining. *Appl. Surf. Sci.* **2002**, *187*, 291−296.
(40) Beamson, G.; Briggs, D. *High Resolution XPS of Organic PolymersThe Scienta ESCA300 Database;* John Wiley and Sons: Chichester, U.K., 1992.